PBAF regulates compartmentalization of actively transcribing chromatin hubs

Charles A. Kenworthy[1], Shu-Hao Liou[1], Panagiotos Chandris[2], Vincent Wong[1], Patrycja Dziuba[1], Luke D. Lavis[3], Wei-Li Liu[1], Robert H. Singer[1,3], and Robert A. Coleman[1*]

[1]Gruss-Lipper Biophotonics Center, Department of Anatomy and Structural Biology, Albert Einstein College of Medicine, Bronx, New York 10461, USA

[2]Section on High Resolution Optical Imaging, National Institute on Biomedical Imaging and Bioengineering, National Institutes of Health, Bethesda, Maryland, 20892, USA

[3]Janelia Research Campus, Howard Hughes Medical Institute, Ashburn, Virginia, 20147

*To whom correspondence should be addressed.
Gruss-Lipper Biophotonics Center, Department of Anatomy and Structural Biology, Albert Einstein College of Medicine, Bronx, NY 10461 Tel: 718-430-8623; Email: robert.coleman2@einstein.yu.edu

Running Title: PBAF's dynamic chromatin targeting for genome organization

Keywords: PBAF, chromatin remodeling, Histone acetylation, Histone H3.3, Single Molecule Tracking, bromodomain, nuclear compartments, hubs

Abstract

Transcriptionally active genes contain acetyl-rich chromatin and are organized in distinct nuclear compartments that are spatially separated from transcriptionally inactive genes. It is not known how this compartmentalized acetylated chromatin is targeted and regulated by chromatin remodelers such as PBAF. Thus, we sought to understand how PBAF targets chromatin and modulates compartmentalization of transcriptionally active genes using live-cell single molecule fluorescence microscopy. Our work reveals chromatin hubs throughout the nucleus where PBAF cycles on and off the genome. Deletion of PBAF's bromodomains impairs recognition of hubs and cycling on chromatin. Interestingly, markers for transcriptionally active and inactive genes can be found in compartments harboring acetylated chromatin at the periphery that is selectively recognized by PBAF via bromodomains. Defects in PBAF's peripheral targeting lead to a select reduction in the size and number of compartments containing transcriptionally active genes. Our data, combined with previous work in Yeast and Drosophila, suggest that PBAF activity serves as a barrier to heterochromatin spreading. Overall, our findings suggest that chromatin compartments are highly structured with unique peripherally associated acetylation marks. PBAF utilizes these marks to help shape nuclear compartments containing transcriptionally active genes, thereby aiding genomic organization.

Introduction

Hi-C studies have shown that genomic regions spanning up to a megabase, contain transcriptionally active genes rich in acetylated chromatin that are grouped together in "A" compartments[1,2]. Neighboring "B" compartments contain inactive chromatin with repressive epigenetic marks and are segmented away from A compartments[2]. High resolution Hi-C maps further identified a second level of local genome organization consisting of topologically associated domains (TADs) spanning sub-megabase regions and loop domains. High-resolution imaging using DNA-FISH in fixed cells has also spatially identified distinct active and inactive compartments that corresponded with genomic studies[3,4].

A number of recent genomic studies have linked dynamic changes in genome topology with chromatin states and gene regulation during cellular stress, cell reprogramming and viral infection[5-7]. Specifically, transcription factor binding and expression of stress response and developmentally regulated genes are often linked to A/B compartment switching at the end of these genes and boundaries between select TADs[5-7]. However, it is unclear how transcription factors dynamically recognize and alter these A/B compartment boundaries to regulate genome topology at the single cell level.

PBAF, an ATP dependent chromatin remodeling complex, regulates transcription of stress response genes in Humans, C. elegans and Yeast via bromodomain dependent targeting of acetylated chromatin at promoters[8-10]. The yeast homolog of PBAF, RSC, has also been shown to alter genome topology likely via modulation of chromatin state and transcription at genes within the boundaries between chromatin domains[11]. Therefore understanding how PBAF dynamically recognizes different chromatin states in genomic

86 compartments in vivo may lead to a greater understanding of the spatial and dynamic
87 regulation of transcription and genome topology.

88 Recent live-cell imaging studies indicate that a number of transcription factors (e.g.
89 RNA Polymerase II, Mediator and Sox2) dynamically bind chromatin as clusters to form
90 hubs that regulate local gene expression[12-17]. However, such dynamic activity of
91 transcriptional regulators, including chromatin modifiers, within distinct chromatin
92 compartments is currently poorly characterized due to a number of technical limitations.
93 In particular, researchers lack efficient methods to identify and quantitatively characterize
94 chromatin in active/inactive compartments in live cells.

95 To spatially distinguish and characterize different chromatin compartments in
96 vivo, we used live cell Single Molecule Tracking (SMT) to dynamically map genomic
97 binding of PBAF alongside markers of transcriptionally active (H3.3) and inactive (HP1α)
98 genes. Our dynamic imaging studies reveal small hubs where PBAF cycles on and off
99 chromatin, which can be further grouped to form large compartments. We next sought to
100 address the pivotal question of how distinct compartmentalized chromatin states are
101 targeted by PBAF. Thus, we investigated PBAF's spatial distribution, velocities and
102 stability on chromatin when encountering H3.3 and HP1α marked compartments. More
103 importantly, we have assessed the role of PBAF's bromodomains in hub targeting,
104 cycling on chromatin, select compartment engagement and genomic organization.
105 Overall, our studies provide new insights into dynamic chromatin targeting of PBAF via
106 bromodomains, which regulates compartmentalization of transcriptionally active genes to
107 aid in genomic organization.
108

Results

PBAF targets chromatin in distinct nuclear hubs and compartments

Active genomic compartments are enriched in acetylated chromatin and transcriptionally active genes[1,18]. PBAF targets a variety of acetylated residues, including H3K14ac and H3K27ac, on chromatin via its 8-12 bromodomains based on *in vitro* studies[19,20]. Therefore, we hypothesized that PBAF would dynamically localize to discrete nuclear compartments that were enriched in acetylated chromatin *in vivo* (Figure 1a).

To characterize the dynamic binding of PBAF to chromatin *in vivo*, we chose to fluorescently tag the BAF180 subunit (i.e. Halo-BAF180 WT, Figure S1), since it harbors six bromodomains critical for interaction with acetyl-lysine residues on histones[21,22]. Motion Blur HILO microscopy combined with live-cell Single Molecule Tracking (SMT) [23] was used to dynamically detect PBAF molecules stably bound to chromatin (Figure 1b and Supplemental Movie S1). At long camera exposure rates (~500 ms), fast-diffusing nuclear PBAF complexes are blurred out and cannot be localized. Single PBAF molecules, stably bound to chromatin targets, appear as distinct Point Spread Functions (PSFs) that can be spatially and temporally resolved (Figure 1b). PSFs, representing PBAF's binding and unbinding on chromatin, appear and disappear stochastically throughout the time course of imaging (Figure 1b and Supplemental Movie S1). We confirmed that these Halo-tagged BAF180 proteins were incorporated into the large multi-subunit PBAF complex via co-immunoprecipitation studies and live-cell fast diffusion measurements (Figures S1 and S2).

131 Two dimensional (2D) projection maps showed select nuclear regions that contained
132 high densities of PBAF's chromatin binding events alongside deserts devoid of binding
133 (Figures 1c, left panel, and S3c). Based upon these maps, we hypothesized that PBAF's
134 distinct localization pattern was due, in part, to dynamic interactions between PBAF's
135 bromodomains and acetylated chromatin. Therefore, we developed an approach to
136 spatially define the frequency of PBAF's chromatin binding within nuclear subregions.
137 These dynamic binding frequency heat maps were generated by raster scanning across the
138 nucleus and counting the number of PBAF-chromatin binding events in a given sized
139 window (binding events/μm^2/sec) (Figures 1c and 1d). Spatially isolated regions
140 representing high frequency PBAF binding to chromatin were scattered throughout the
141 nucleus (Figure 1d, yellow spanning to red regions).

142 Analysis with the smallest scanning window (0.064 μm^2) revealed hubs of repeated
143 PBAF binding events to target loci within an area of ~250 nm in diameter (Figure 1d, top
144 panel). Importantly, no hubs were detected in simulations where localizations of an
145 equivalent number of binding events were randomized throughout the nucleus (Figure
146 S4a). These results are consistent with previous studies showing hubs of EWS/FLI1,
147 Sox2 and RNA Polymerase II at enhancers and promoters in nuclear domains of roughly
148 equivalent sizes[13,14,16,24]. Therefore, we speculate that these PBAF hubs represent
149 repeated binding or "cycling" on nucleosomes in small genomic regions at enhancers and
150 promoters.

151 The largest scanning window (2.54 μm^2) indicated clusters of binding hubs grouped
152 together to form a large compartment (~1.7 μm in diameter, Figure 1d, right panel).
153 Importantly, the average size of our PBAF binding compartments in live cells was only

154 slightly larger than active and inactive chromatin compartments measured by super-
155 resolution microscopy in fixed cells[4]. Overall, these results suggest that PBAF is likely
156 targeting chromatin in a permissive state over select genomic regions that are packaged in
157 confined hubs that are grouped in compartments.

158 **PBAF targeting and cycling on chromatin hubs is regulated by BAF180**
159 **bromodomains**

160 It is generally thought that arrays of acetylated nucleosomes are repeatedly targeted
161 by bromodomain containing chromatin remodeling complexes such as PBAF (Figure
162 2a)[25]. Multiple PBAF subunits contain bromodomains that recognize a large variety of
163 acetyl-lysine residues in chromatin[20,26-28]. Notably, BAF180 contains six bromodomains
164 while BRG1 and BRD7 each contain one bromodomain. Therefore, we hypothesized that
165 BAF180 bromodomains would have major role in PBAF's targeting and cycling on hubs
166 (Figure 2a).

167 To determine if chromatin hubs were targeted via PBAF bromodomain/acetyl-lysine
168 interactions, we compared the high frequency binding of wild-type PBAF and a mutant
169 PBAF lacking the six BAF180 bromodomains (i.e. ΔBD) (Figure 2b). Interestingly, the
170 number of PBAF binding hubs in each cell was reduced upon deletion of BAF180
171 bromodomains (Figure 2c). Correspondingly, the number of PBAF binding hubs
172 increased in a BAF180 bromodomain-dependent manner when global levels of histone
173 acetylation were elevated via SAHA treatment (Figures 2c and S4b). Overall, our data
174 indicate that target hubs are defined by repeated rounds of PBAF binding to chromatin
175 via BAF180 bromodomains/acetyl-lysine interactions.

176 We next investigated how chromatin in target hubs is temporally occupied by PBAF.
177 Chromatin hubs are occupied via a series of PBAF binding and unbinding events
178 interspersed with latent periods of non-occupancy (Figure 2d). We found that both wild-
179 type PBAF and mutant PBAF ΔBD, on average, exhibited ~9-10 rounds of repeated
180 binding at target hubs over ~18 minutes of continuous imaging (Figure 2e). Furthermore,
181 elevated histone acetylation levels led to a slight but significant increase in the number of
182 PBAF binding cycles at target hubs for both wild-type and mutant PBAF (Figure 2e). We
183 speculate that residual bromodomains in mutant PBAF's BRD7 and BRG1 subunits may
184 compensate to increase cycling on select arrays of hyperacetylated nucleosomes.

185 To assess further assess the molecular origins of cycling on chromatin hubs,
186 histograms of PBAF latency times were generated and fit to single, double and triple
187 exponential decay models (Figure S4b). Statistical analysis indicated that a triple
188 exponential decay model best fit the distribution of PBAF latency times. This enabled us
189 to classify latency times as either short (~4.5 sec), intermediate (~21 sec) or long (~205
190 sec) (Figure S4b). Removal of BAF180 bromodomains altered PBAF's latency at hubs
191 (Figures 2f and S4d), specifically increasing the long latency time of mutant PBAF
192 cycling events (compare WT vs ΔBD). Notably, this difference in latency between wild-
193 type and mutant PBAF was also further enhanced on hyperacetylated chromatin (Figure
194 2f, SAHA treatment). Therefore, PBAF's cycling and re-occupancy of acetylated
195 chromatin hubs may be aided via BAF180 bromodomains.

196 **Dynamic mapping of PBAF, transcriptionally active and heterochromatic**
197 **compartments**

198 Thus far, our dynamic binding frequency heat maps allow us to quantitate PBAF
199 target hubs grouped in close proximity (Figure 1d). We have termed these grouped hubs
200 as PBAF binding compartments given their large size and distinct localization patterns
201 (Figures 1d and 3a). Previous studies have established that PBAF binds nucleosomes at
202 promoters of both transcriptionally active and repressed genes[19,29-32]. To test if PBAF
203 localizes on chromatin in different compartment types, we used a similar strategy as
204 above to dynamically image transcriptionally active (H3.3-SNAP) and heterochromatic
205 (SNAP-HP1α) nuclear subregions in single cells (Supplemental Movies S2 and S3).
206 Compartments containing dense high frequency H3.3-SNAP genomic interactions were
207 found within distinct subregions in the nucleus (Figure 3b, left panel). Likewise,
208 heterochromatic compartments harboring high frequency SNAP-HP1α/chromatin
209 interactions were also observed (Figure 3b, right panel). HP1α compartments defined in
210 this manner roughly resembled the size of phase-separated heterochromatin[33]. These
211 results demonstrate that we can identify large transcriptionally active and inactive regions
212 of the genome clustered in select compartments in a live cell.

213 Our analysis allows us to quantitate the number and sizes of compartments in a
214 single cell. Interestingly, the number of PBAF compartments was reduced with a minimal
215 impact on their size in our mutant PBAF ΔBD expressing cells (Supplemental Figures
216 S5a and S5b). These results suggest that a subset of PBAF compartments is defined via
217 BAF180 bromodomain targeting to select acetylation marks in chromatin hubs. We also
218 found that the number and size of the H3.3 compartments were significantly diminished
219 in our mutant PBAF BAF180 ΔBD cells (Figures 3c and 3d). Therefore, PBAF may be
220 regulating the establishment of a subset of H3.3 compartments. Moreover, there were no

221 differences in the number and size of HP1α compartments between wild-type and mutant
222 PBAF cells (Figures 3c and 3d). Overall, our results suggest that establishment of H3.3
223 compartments, in part, requires PBAF's BAF180 bromodomains.

224 **Select spatial targeting of chromatin in transcriptionally active and heterochromatic**
225 **compartments**

226 To further reveal any spatial correlations between different compartments, dual color
227 single molecule imaging was performed to map PBAF's binding to chromatin alongside
228 transcriptionally active or inactive compartments inside a single cell (Figure 4). First, we
229 observed some high frequency PBAF binding that overlapped with both transcriptionally
230 active and heterochromatic compartments (Figure 4a). In terms of total compartment area,
231 approximately 27% and 24% of our mapped PBAF compartments overlapped
232 respectively with the H3.3 and HP1α compartments (Figure 4b). Collectively, over 50%
233 of the total area of PBAF's compartments coincide with compartments containing H3.3
234 and HP1α marked chromatin. We surmise that the chromatin within the remaining non-
235 overlapping regions of PBAF compartments might be associated with additional subtypes
236 of inactive compartments not marked by HP1α[2].

237 Next, to better characterize chromatin states within compartments, PBAF SMT
238 trajectories within H3.3 or HP1α compartments were isolated (Figures S6a and S6b).
239 Roughly 23% and 21% of PBAF's total nuclear chromatin binding events respectively
240 occurred within transcriptionally active H3.3 or HP1α marked compartments (Figure 4c).
241 Notably, upon close inspection, a large number of PBAF's chromatin binding events
242 localized to the periphery of H3.3 or HP1α marked compartments (Figure 4d).

243 To quantitatively determine PBAF's preferential targeting inside compartments, we
244 examined the ratio between the number of PBAF binding events inside of compartments
245 (nPBIC) and the area of compartments (nAC, see methods). A value greater than 1 for the
246 nPBIC/nAC ratio indicates enrichment of PBAF binding inside a specific type of
247 compartment relative to global chromatin. A value less than 1 for the nPBIC/nAC ratio
248 indicates depletion of PBAF binding inside compartments. Overall, we observed an
249 enrichment of PBAF binding inside the H3.3 and HP1α compartments (i.e. Entire Comp.
250 shown in Figure 4e, top panels).

251 To pinpoint where PBAF was mostly enriched inside compartments, we then plotted
252 nPBIC/nAC ratios as a function of PBAF's distance away from the compartment
253 periphery (Figure 4e). We found a significant differential enrichment of wild-type
254 PBAF's chromatin binding within ~84 nm of the periphery inside of H3.3 and HP1α
255 compartments (top panels). In stark contrast, mutant PBAF that lacks BAF180
256 bromodomains (i.e. ΔBD) displayed no spatial enrichment close to the periphery of H3.3
257 and HP1α compartments (bottom panels). Thus, these findings reveal that chromatin at
258 the edge of both transcriptionally active and heterochromatic compartments likely
259 contains distinct acetylation marks that target PBAF via BAF180 bromodomains.

260 To support our live-cell dynamic tracking of PBAF binding on select distinct
261 chromatin, super-resolution STORM microscopy in fixed cells was also conducted
262 (Figure S7). The analysis validates the overlap between wild-type PBAF and H3.3/HP1α
263 marked chromatin (Figure S7, cyan). In many subnuclear regions, PBAF binds chromatin
264 and forms a distinct close interface surrounding H3.3 marked chromatin domains (Figure
265 S7, bottom left panel, highlighted in red stars), consistent with the results in Figure 4. A

266 similar but less pronounced pattern was seen with PBAF and HP1α marked chromatin
267 domains (Figure S7, bottom right panel). Taken together, these studies illustrate that
268 PBAF can selectively bind distinct transcription-regulated chromatin via BAF180's
269 bromodomains.

270 **Transcriptionally active versus heterochromatic chromatin is differentially engaged**
271 **by PBAF**

272 Chromatin states are thought to significantly differ between transcriptionally active
273 and heterochromatic compartments[1,18]. To further characterize these different chromatin
274 states, we determined PBAF's genomic residence time in transcriptionally active H3.3
275 and heterochromatic HP1α compartments (Figure 5a). Residence time analysis revealed
276 two chromatin-binding populations of PBAF in a representative H3.3 compartment
277 (Figure 5b, red line). The predominant PBAF population (~83% of molecules) transiently
278 bound chromatin for ~0.8 seconds. This PBAF population most likely represents non-
279 specific binding since residence time analysis for the Halo-tag alone also showed brief
280 (0.8 sec) interactions with chromatin[23]. The remaining PBAF molecules (~17%) stably
281 bound to chromatin in this H3.3 compartment for ~9 seconds on average. Importantly, we
282 are measuring PBAF's dissociation from chromatin, as its residence time (9 sec) is
283 significantly shorter than our dye photobleaching rates ($t_{1/2}$ of approximately 100-200
284 sec).

285 PBAF's residence time broadly varied from ~7-22 seconds within different H3.3
286 compartments in the same cell (Figure 5c). Global analysis reveals two subclasses of
287 H3.3 compartmentalized chromatin across different cells that are targeted by PBAF
288 (Figure 5d, green line). PBAF bound to chromatin for ~8 seconds in the majority of H3.3

289 compartments, with a minor population of compartments exhibiting a residence time of
290 16 seconds. Comparatively, there was only one class of heterochromatic HP1α
291 compartments displaying an average PBAF residence time of ~12 seconds on chromatin
292 (Figure 5d, red line). Overall, the majority of PBAF molecules that localized to H3.3
293 marked chromatin bound for a shorter duration than tracks within HP1α regions (Figure
294 5d). These results indicate that our dynamic imaging can segment compartments
295 containing different chromatin states. Furthermore, this underlying chromatin state of
296 target nucleosomes in different compartments affects PBAF's binding.

297 To assess if BAF180 bromodomains regulate PBAF's stability on chromatin, we
298 examined the residence time of mutant PBAF ΔBD on chromatin globally (Figure S8)
299 and in compartments (Figure 5e). Mutant PBAF ΔBD had a decreased percentage of
300 stable global chromatin binding events, indicating an inefficient target search mechanism
301 (Figure S8a). Compared to wild-type PBAF, mutant PBAF ΔBD had reduced residence
302 times on chromatin globally (Figure S8b) and in high frequency PBAF compartments
303 (Figure S8c). Thus, PBAF lacking BAF180 bromodomains has defects in associating
304 with and anchoring to chromatin. Intriguingly, while there was a significant reduction in
305 stability on global chromatin, mutant PBAF ΔBD exerted little difference in residence
306 times between transcriptionally active H3.3 and heterochromatic HP1α compartments
307 (Figure 5e). Notably, PBAF ΔBD exhibited a bimodal distribution profile of residence
308 times (~8 and ~13 sec) within heterochromatic HP1α compartments. Therefore, a
309 subclass of distinct heterochromatic compartments is defective for interacting with PBAF
310 ΔBD (~8 sec) compared to PBAF WT (residence time ~12 sec, Figure 5d versus 5e). We
311 speculate that PBAF may target at least two different types (i.e. BAF180 bromodomain

312 dependent and independent) of HP1α-marked heterochromatic compartments via distinct
313 subunits and mechanisms.

314 **Surveying the local chromatin environment of PBAF target loci**
315
316 ATP-dependent nucleosome remodelers, such as PBAF, are known to reposition
317 nucleosomes along the DNA[34,35]. In the cell, PBAF's movement when bound to a
318 genomic scaffold could be due to (1) translocation along the DNA, (2) local constrained
319 diffusion of the genomic DNA that is dependent on local chromatin density, or (3) a
320 combination of both translocation and DNA diffusion. Regardless of its origin, we
321 surmised that PBAF's movement could serve as a probe of the local condensation status
322 of chromatin (Figure 6a). Thus, we hypothesized that PBAF would move faster when
323 bound to nucleosomes within open euchromatic versus condensed heterochromatic loci
324 (Figure 6a).

325 To study PBAF's movement on chromatin, we measured the frame-to-frame X, Y
326 positional displacements of individual genome bound PBAF SMT trajectories (Figure 6b).
327 Interestingly, both unfiltered (thin blue/yellow lines) and smoothed (thick dark blue and
328 orange lines) SMT trajectories of chromatin bound PBAF predominantly displayed
329 asymmetric elongated curvilinear movement (Figure 6b). This movement was not due to
330 cell migration or microscope drift as trajectories occurring in close spatial and temporal
331 proximity often moved in opposing or distinct directions. Our results were consistent
332 with previous studies showing that chromatin moves via a curvilinear mechanism[36,37].

333 We next sought to address whether different chromatin states of target
334 nucleosomes would impact PBAF's velocity. To begin tackling this task, we
335 quantitatively characterized the movement of individual trajectories (Figure S9a). The

336 velocity of PBAF's curvilinear movement was discontinuous, occurring in a series of
337 starts and stops. Furthermore, multiple Gaussian model fitting of the individual
338 trajectory's average velocities revealed at least three to four distinct populations of PBAF
339 velocities (Figure 6c). These four populations may reflect four different chromatin states
340 bound by PBAF. For clarity, we combined the two fast PBAF movement populations into
341 a single category. We suspected that less crowded euchromatic loci would allow fast
342 movement of PBAF (Figure 6a, left panel). Correspondingly, heterochromatin would
343 result in medium and slow moving PBAF (Figure 6a, right panel). Notably, throughout
344 the nucleus, approximately 77% of PBAF's global chromatin binding events displayed
345 medium and slow velocities on chromatin (Figure 6c). This suggests that the majority of
346 chromatin throughout the nucleus is in a densely packed heterochromatic state (Figure 6a,
347 right panel).

348 Next, we compared PBAF's movement when bound to H3.3 versus HP1α marked
349 chromatin (Figure 6d). HP1α marked chromatin compartments contain a significantly
350 higher percentage of slow moving PBAF relative to H3.3 containing chromatin.
351 Correspondingly, open euchromatic H3.3 marked chromatin harbors an elevated
352 percentage of fast moving PBAF molecules versus condensed heterochromatic loci
353 (Figure 6d), likely reflecting differences in the local nucleosome density surrounding
354 target loci.

355 Throughout the nucleus, global chromatin is relatively closed and thought to
356 contain predominantly the histone H3.1 variant in place of H3.3[38]. Therefore, as a control,
357 we further examined PBAF's velocity outside of H3.3 marked compartments. Indeed,
358 there was an increased percentage of slow moving wild-type PBAF bound to H3.1

359 marked chromatin outside of H3.3 marked compartments (i.e. 37% vs. 21%, Figures S9b
360 and 6d). On the other hand, we observed a decrease in the slow moving PBAF population
361 outside of HP1α marked compartments (i.e. 35% vs. 42%, Figure S9b and 6d). This
362 suggests that the global chromatin on average is slightly less densely packed compared to
363 HP1α marked chromatin. Collectively, PBAF's differential velocities likely reflect
364 chromatin compaction, which increases from H3.3 to H3.1 to HP1α marked chromatin
365 states. However, we can't exclusively rule out the possibility that PBAF may bind these
366 distinct types of chromatin via different mechanisms and subunits, resulting in distinct
367 velocities regardless of compaction states.

368 Residence time analysis indicated that removal of PBAF's bromodomains altered
369 binding in heterochromatic compartments (Figure 5e). Therefore, we exploited mutant
370 PBAF ΔBD's velocity to infer the local chromatin density of its targets within
371 heterochromatin. Interestingly, we observed a decreased percentage of slow moving
372 mutant PBAF ΔBD molecules relative to wild-type PBAF in heterochromatic HP1α
373 compartments (Figure 6d). It is important to note that these results are consistent with the
374 residence time analysis (Figures 5d and 5e), implying mistargeting of mutant PBAF ΔBD
375 to potentially unstable nucleosomes within heterochromatic compartments. Taken
376 together, our studies suggest that PBAF uses bromodomains for targeting distinct
377 chromatin states within heterochromatic compartments.
378

379 **Discussion**

380 A battery of work has now established that transcriptionally co-regulated genes
381 are clustered in compartments containing Topologically Associated Domains (TADs) or
382 transcription factories in the nucleus (Figure 1a)[1,13,18,39]. However, little is known about
383 how these compartments are dynamically targeted and shaped by chromatin modifiers.
384 We proposed that PBAF could act to remodel chromatin in promoters, enhancers and
385 boundary elements in distinct subnuclear compartments. Using dynamic live-cell single
386 molecule tracking, chromatin binding frequency heat maps allowed us to visualize
387 compartmentalized chromatin binding of PBAF at different scales dependent on the size
388 of our scanning window (Figure 1d). As expected, different chromatin interacting
389 proteins, such as the H3.3 histone variant and the HP1α heterochromatic binding protein,
390 also displayed compartmentalized binding in our live-cell imaging analysis (Figure 3b).
391 Therefore, we and other research groups have established that dynamic single molecule
392 tracking is useful for identifying and characterizing compartmentalized genomic binding
393 of a broad range of nuclear factors[16,17].

394 Large chromatin domains (~2-30 kb) can be found to be acetylated throughout the
395 genome [40,41]. We proposed that the discrete PBAF hubs identified in our heat maps
396 (Figure 1d) represent repeated binding to arrays of closely spaced acetylated nucleosomes
397 during our live-cell imaging (Figure 2). Indeed, removal of BAF180's bromodomains
398 reduced the number of PBAF hubs, while elevated global histone acetylation increased
399 the number of hubs (Figure 2c). Therefore, we surmise that PBAF binding hubs represent
400 acetylated loci (Figure 7a). Interestingly, our latency analysis reveals that BAF180
401 bromodomains also increase PBAF cycling on acetylated chromatin in hubs (Figure 2f).

402 Therefore, our studies support that PBAF utilizes bromodomain/acetyl interactions to
403 remain in the immediate vicinity of target chromatin, likely facilitating repeated rounds
404 of remodeling events on nucleosomal arrays (Figures 2a and 7a).

405 Our data visualized large compartments encompassing grouped hubs of
406 transcriptionally active genomic regions (Figure 3b, left panel). This result complements
407 Hi-C genomic studies[1,18], indicating that compartmentalized regions of the genome
408 contain acetylated histone marks associated with active transcription. Notably, formation
409 of transcriptionally active compartments is likely regulated via PBAF's peripheral
410 targeting of acetylated chromatin (Figures 3c, 3d, 4d, 4e and 7b). We speculate that
411 reduced targeting of mutant PBAF ΔBD away from the periphery may lead to enhanced
412 heterochromatic spreading decreasing both the size and number of transcriptionally active
413 compartments (Figures 3c and 3d). Our findings are consistent with BAF180's role in
414 promoting H3.3 loading during the formation of functional boundary elements to prevent
415 pericentric heterochromatin spreading in Drosophila[42]. In addition, RSC, the yeast
416 homolog of PBAF, is known to play a major role in establishment of nucleosome free
417 regions at the boundaries of chromatin interaction domains leading to a less compact
418 genome[11]. Therefore PBAF may have conserved role in shaping genome topology via
419 prevention of heterochromatic spreading into compartments containing transcriptionally
420 active genes.

421 Previous studies have focused on the ability of PBAF and related chromatin
422 remodeling complexes to strictly engage facultative heterochromatin and antagonize
423 Polycomb mediated repression[43,44]. Our data indicate that PBAF also functions at the
424 periphery of constitutive HP1α marked heterochromatic compartments (Figure 4a, right

425 panel). Reports documented that the BRG1 subunit of PBAF binds to HP1α and is
426 required for loading of HP1α onto heterochromatin *in vitro* and *in vivo*[45,46]. HP1α
427 prevents spreading of H3K27me^3, a well-known target of Polycomb, in pericentric
428 heterochromatin[47]. We speculate that PBAF aids heterochromatic loading of HP1α at the
429 periphery of constitutive heterochromatic compartments to disrupt spreading of
430 H3K27me^3 and antagonize Polycomb binding. Therefore, our studies uncover a novel
431 role for PBAF in chromatin remodeling of HP1α marked heterochromatic regions.

432 Different chromatin states can be, in part, defined by their nucleosome stability[48].
433 Thus, different chromatin states may also be reflected by the genomic residence time of
434 chromatin remodelers in a live cell. Our imaging experiments support this idea by
435 showing that PBAF displayed shorter residence times in H3.3 marked transcriptionally
436 active regions compared to HP1α containing heterochromatic regions (Figure 5d). This is
437 completely consistent with previous in vitro and in vivo studies showing inherent
438 instability of H3.3 containing nucleosomes[49-51]. Thus, rapid turnover of PBAF's
439 chromatin occupancy in transcriptionally active regions may directly reflect nucleosome
440 stability (Figure 7b), which could help define different chromatin states.

441 Time-dependent averaging of PBAF chromatin binding trajectories revealed
442 directional movement (Figure 6b). Furthermore, there is a strong correlation between
443 chromatin structure and PBAF's velocity (Figure 6d), with complexes moving slower as
444 nucleosome density increases (Figure 7b). Surprisingly, mutant PBAF lacking BAF180
445 bromodomains moved faster compared to wild-type PBAF in HP1α marked
446 heterochromatic compartments (Figure 6d). Thus, our data indicate that mutant PBAF
447 ΔBD may be mistargeted to distinct local heterochromatin environments containing less

448 densely packed nucleosomes. This is further supported by data showing that mutant
449 PBAF ΔBD binds for shorter periods of time relative to wild-type PBAF in HP1α marked
450 heterochromatic compartments (Figure 5d vs 5e). Alternatively, it is also possible that
451 different subunits and mechanisms, independent of chromatin compaction states, regulate
452 mutant PBAF ΔBD's velocity on heterochromatin.

453 Thus far, numerous research groups have uncovered a plethora of histone post-
454 translational marks (PTM) utilized by chromatin remodelers to regulate transcriptional
455 activation[52]. Previous genomic studies have mapped these histone acetylation marks to
456 broad chromatin domains along with select regions of promoters and enhancers[40,41,53].
457 Recent studies on 3D organization of the genome revealed compartments containing
458 histone marks associated with activated transcription[18,54]. By characterizing the dynamic
459 genomic binding of PBAF, which recognizes many of these acetylation marks, our work
460 helps to define the spatial and temporal histone modification of chromatin hubs and
461 compartments. Future live-cell single molecule imaging studies of additional histone
462 PTM writers, readers, and the histone marks themselves will shine new light on the
463 spatiotemporal organization of the 4D epigenome.
464

465 **Methods**

466 **Plasmid constructions, biochemistry and generation of cell lines**

467 Details of plasmid construction, biochemical analysis of Halo-BAF180 and
468 generation of cell lines are described in the Supplemental Methods section.

469 **Live-cell fluorescent labeling of Halo-BAF180 WT and Halo-BAF180 ΔBD**

470 Cells stably expressing Halo-BAF180 WT were grown to a density of ~$5x10^5$
471 cells on 35 mm MatTek imaging dishes. Twenty-four hours prior to transfection of Halo-
472 BAF180 ΔBD, parental U2OS cells were grown to a density of ~$1x10^5$ cells in 35 mm
473 MatTek imaging dishes. Cells were then transiently transfected with the pFRT-Halo-
474 BAF180 ΔBD plasmid and incubated overnight prior to further treatments.

475 Twenty-four hours before labeling, cells were treated with either 2.5 μM SAHA
476 (Cayman Chemical) or matching vehicle control (DMSO, 0.25% final concentration)
477 (Sigma) and were incubated at 37°C with 5% CO_2. Immediately prior to imaging, cells
478 were incubated with 0.4 nM JF549-HTL dye for 15 minutes at 37°C. Cells were then
479 washed 3 times with 1X PBS, replaced with complete DMEM and incubated for 30
480 minutes at 37°C to remove unincorporated dye. Cells were then washed 2 times with 1X
481 PBS and placed in L-15 imaging media (Life technologies) + 10% FBS for imaging.

482 **Dual color live-cell fluorescent labeling of Halo-BAF180 WT/ΔBD and H3.3-SNAP**
483 **or SNAP-HP1α**

484 Cells stably co-expressing Halo-BAF180 WT along with either H3.3-SNAP or
485 SNAP-HP1 were grown to a density of ~$5x10^5$ cells on 35 mm MatTek imaging dishes.
486 Immediately prior to imaging, cells were incubated with 10 nM SNAP-Cell 647-SiR
487 (New England Biolabs) and 0.4 nM JF549-HTL at 37°C for a total of 30 and 15 minutes,

488 respectively. Cells were then washed 3 times with 1X PBS, replaced with complete
489 DMEM and further incubated for 30 minutes at 37°C to remove unincorporated dye.
490 Cells were then washed 2 times with 1X PBS and placed in L-15 imaging media (Life
491 technologies) + 10% FBS for imaging. Two color labeling of Halo-BAF180 ΔBD along
492 with H3.3-SNAP or SNAP-HP1α was performed as described above, except that Halo-
493 BAF180 ΔBD were electroporated with pSNAP plasmids 24-72 hours prior to labeling.

494 **Live-cell single molecule imaging of Halo-BAF180 WT/ΔBD, H3.3-SNAP or SNAP-**
495 **HP1α**

496 All imaging sessions were carried out at room temperature. Cells were
497 continuously illuminated using a 532 nm (13 W/cm^2, Coherent) or 640 nm (9.5 W/cm^2,
498 Coherent) laser for JF549-HTL and SNAP-Cell 647-SiR imaging respectively. Time-
499 lapse two-dimensional (2D) images of single molecules were acquired with a customized
500 inverted Nikon Eclipse Ti microscope with a 100X oil-immersion objective lens (Nikon,
501 1.49 NA) and further magnified 1.5X post-objective. BAF180 images were acquired at 2
502 Hz for ~18 minutes using an EMCCD (iXon, Andor) with a 512 x 512 pixel field of view
503 (final pixel size of 84 nm). SNAP imaging proceeded at 2 Hz for ~4.5 minutes in cells
504 that also expressed either SNAP-Cell 647-SiR labeled H3.3-SNAP or SNAP-HP1α.

505 **Image Processing and single molecule tracking**

506 Movies of acquired images were processed to subtract background in ImageJ
507 using a rolling ball radius of 50 pixels. Background subtracted movies were subjected to
508 Multi-Target Tracking (MTT) to resolve the trajectories of individual molecules [55] using
509 a GUI based implementation, SLIMfast [56]. Localization of individual molecules was
510 achieved by fitting Point Spread Functions (PSFs) of discrete single spots with a 2D

511 gaussian function. Tracking of single molecule chromatin binding events was performed
512 by connecting BAF180 localizations between consecutive frames. Tracking was based
513 upon a maximum expected diffusion constant of 0.05 μm^2/second and allows for 1.5
514 second gaps in trajectories due to blinking or missed localizations. Track positions from
515 individual trajectories were averaged to generate a 2D projection map of BAF180 binding
516 events over 18 minutes of imaging.

517 Nuclear BAF180 tracks were identified based on the boundaries from 2D
518 projection maps of 180 binding events. BAF180 tracks that fell outside of the nucleus
519 were excluded. Photobleach rates were then determined for each background-subtracted
520 movie based upon exponential decay of the global fluorescence of chromatin bound
521 Halo-BAF180 WT/ΔBD, H3.3-SNAP, SNAP-HP1α.

522 **Analysis of PBAF chromatin binding residence times**

523 Chromatin binding residence time was determined by plotting a survival curve (1-
524 Cumulative Density Function, 1-CDF) of the track-lengths of chromatin bound Halo-
525 BAF180 in each cell. Single and double-exponential models were then fitted to these 1-
526 CDF plots to determine residence times. One-way ANOVA followed by Tukey's post-
527 hoc t-tests were performed to determine pairwise significance of global residence times
528 and percentages of stable PBAF binding events.

529 **Analysis of PBAF clustering in hubs**

530 2D projection maps of BAF180 binding events lasting at least one second
531 (Figures 2e and 2g) or eight seconds (Figure 2c) were expanded 10 fold in the X and Y
532 directions yielding a final pixel size of 8.4 nm. Areas of high PBAF binding densities
533 were determined by counting the number of binding events within an octagon window

534 (diameter 168 nm) as it was raster scanned across the nucleus of the expanded 2D
535 projection map. Contiguous octagon widows centered on an individual pixel containing at
536 least 3 PBAF binding events were defined and labeled as hubs. The total number of hubs
537 per cell were then normalized to the total PBAF binding events per cell and multiplied to
538 produce the number of PBAF hubs formed per 10,000 PBAF binding events (i.e. Number
539 of PBAF hubs) for each cell. Overall significance was determined with a two-sample
540 Kruskal-Wallis test to determine pair-wise significance.

541 To quantitate PBAF binding latency times in hubs, tracks of binding events in
542 individual hubs were further analyzed to determine the time periods between single
543 PBAF binding events. 1-CDF survival plots of all PBAF latency times in hubs in a single
544 cell were fit with a single, double, and triple exponential decay model. Overall
545 significance was determined with a two-sample Kruskal-Wallis test to determine pair-
546 wise significance.

547 **Mapping of PBAF binding compartments**

548 Contiguous nuclear regions of compartments containing high frequency PBAF
549 binding in cells were determined by raster scanning of a 19 x 19 pixel (2.54 μm^2) window
550 across the nucleus. Binding events that fell within this window were then counted to
551 generate an overall binding density for individual pixels throughout the nucleus. Pixels in
552 the resulting PBAF density map, which displayed a lower binding density than the
553 average global binding density, were filtered out and eliminated. Remaining continguous
554 areas containing at least 10 pixels displaying a high frequency of PBAF binding events
555 were grouped as compartments. For residence time analysis, compartments with fewer
556 than 120 binding events were eliminated to permit more robust statistical analysis of

557 events. Track lengths for molecules within these remaining compartments were then
558 plotted as a 1-CDF survival curve and fit to single- and double-exponential decay
559 functions. Residence times of the specific binding population for each compartment were
560 plotted as Probability Density Functions (PDF). Statistical differences between genotypes
561 or treatment conditions were then assessed using a two-sample Kolmogorov-Smirnov test.

562 **Characterization of PBAF localization to H3.3 or HP1α compartments**

563 High binding density H3.3 or HP1α compartments were mapped using MTT and
564 raster scanning as described above. Remaining compartments were then filtered, such
565 that regions below a threshold of 0.5% of total nuclear binding events for H3.3 and HP1α
566 were eliminated. PBAF binding events within each compartment were summed and
567 normalized to the total number of PBAF binding events within the cell (nPBIC). This was
568 further normalized to the percentage of the total nuclear area occupied by either H3.3 or
569 HP1α compartments (nAC). For analysis of binding probability in relation to
570 compartment periphery, the number of PBAF binding events within a 1 pixel (84 nm)
571 band around the perimeter of the compartment was determined and normalized to the
572 total number PBAF binding events in the cell. This was further normalized to the
573 percentage of nuclear area occupied by the 1 pixel (84 nm) band around the perimeter of
574 the compartment. The outer band of the compartment was then removed and the
575 subsequent binding probability analysis for the 84-168 nm, 169-252 nm, 253-336 nm,
576 337-420 nm bands away from the compartment periphery were performed in a similar
577 manner. Overall significance was determined with a two-sample Kruskal-Wallis test to
578 determine pair-wise significance.
579

580 **Characterization of PBAF binding dynamics within H3.3 or HP1α compartments**

581 Track lengths for PBAF molecules within compartments were plotted as a 1-CDF
582 survival curve and fit to single- and double-exponential decay functions. Residence times

583 of the specific binding population for each compartment were plotted as Probability
584 Density Functions (PDF). Statistical differences between genotype or treatment
585 conditions were then assessed using a two-sample Kolmogorov-Smirnov test.

586 **Velocity analysis of chromatin bound PBAF**

587 To assess the average velocity of chromatin bound PBAF within compartments
588 (Figure 6), we analyzed PBAF molecules bound between 7.5 and 15 seconds, based on
589 the average residence times of PBAF within H3.3 and HP1α marked compartments
590 (Figures 5d and 5e). Localizations (i.e. X, Y positions) from PBAF binding trajectories
591 (Figure 6b) were time averaged using a top hat filter with a sliding window of 5.5
592 seconds. The distance of the displacement between time-averaged localizations from
593 subsequent frames (0.5 seconds) was then used to generate a velocity for each individual
594 step throughout the binding trajectory (Figure S9a). Velocities throughout the binding
595 trajectory were then averaged to obtain a mean velocity for an individual PBAF
596 chromatin binding event. Histograms of mean PBAF velocities within compartments
597 were then fit using a four component Gaussian mixture model employing an iterative
598 Expectation Maximization algorithm in MATLAB. The resulting Gaussian mixture
599 models revealed populations containing 4 unique subclasses of velocities for PBAF
600 genomic binding events. The data are represented by the mean percentage and standard
601 deviation of each subclass from 50 independent Gaussian mixture models fit to the
602 histograms of PBAF velocities.

603 **Data Availability**

604 Datasets generated in this study are available at the NIH 4D Nucleome Data portal
605 (data.4dnucleome.org) : 4DNES2DS2N1U, 4DNESL67GMLC, 4DNES3RWS1Y5,
606 4DNES6IJ8J3X, 4DNESC234IRM, 4DNESCE4GQDC, 4DNESGYDFIM4, and 4DNESEAOOIOB.
607

608 **References**

609 1 Lieberman-Aiden, E. *et al.* Comprehensive mapping of long-range interactions
610 reveals folding principles of the human genome. *Science* **326**, 289-293,
611 doi:10.1126/science.1181369 (2009).
612 2 Rao, S. S. *et al.* A 3D map of the human genome at kilobase resolution reveals
613 principles of chromatin looping. *Cell* **159**, 1665-1680,
614 doi:10.1016/j.cell.2014.11.021 (2014).
615 3 Bintu, B. *et al.* Super-resolution chromatin tracing reveals domains and
616 cooperative interactions in single cells. *Science* **362**, doi:10.1126/science.aau1783
617 (2018).
618 4 Wang, S. *et al.* Spatial organization of chromatin domains and compartments in
619 single chromosomes. *Science* **353**, 598-602, doi:10.1126/science.aaf8084 (2016).
620 5 Amat, R. *et al.* Rapid reversible changes in compartments and local chromatin
621 organization revealed by hyperosmotic shock. *Genome Res* **29**, 18-28,
622 doi:10.1101/gr.238527.118 (2019).
623 6 Stadhouders, R. *et al.* Transcription factors orchestrate dynamic interplay between
624 genome topology and gene regulation during cell reprogramming. *Nat Genet* **50**,
625 238-249, doi:10.1038/s41588-017-0030-7 (2018).
626 7 Heinz, S. *et al.* Transcription Elongation Can Affect Genome 3D Structure. *Cell*
627 **174**, 1522-1536 e1522, doi:10.1016/j.cell.2018.07.047 (2018).
628 8 Porter, E. G. *et al.* PBRM1 Regulates Stress Response in Epithelial Cells.
629 *iScience* **15**, 196-210, doi:10.1016/j.isci.2019.04.027 (2019).
630 9 Kuzmanov, A., Karina, E. I., Kirienko, N. V. & Fay, D. S. The conserved PBAF
631 nucleosome-remodeling complex mediates the response to stress in
632 Caenorhabditis elegans. *Mol Cell Biol* **34**, 1121-1135, doi:10.1128/MCB.01502-
633 13 (2014).
634 10 Damelin, M. *et al.* The genome-wide localization of Rsc9, a component of the
635 RSC chromatin-remodeling complex, changes in response to stress. *Mol Cell* **9**,
636 563-573 (2002).
637 11 Hsieh, T. H. *et al.* Mapping Nucleosome Resolution Chromosome Folding in
638 Yeast by Micro-C. *Cell* **162**, 108-119, doi:10.1016/j.cell.2015.05.048 (2015).
639 12 Cho, W. K. *et al.* RNA Polymerase II cluster dynamics predict mRNA output in
640 living cells. *Elife* **5**, doi:10.7554/eLife.13617 (2016).
641 13 Cisse, II *et al.* Real-time dynamics of RNA polymerase II clustering in live
642 human cells. *Science* **341**, 664-667, doi:10.1126/science.1239053 (2013).
643 14 Liu, Z. *et al.* 3D imaging of Sox2 enhancer clusters in embryonic stem cells. *Elife*
644 **3**, e04236, doi:10.7554/eLife.04236 (2014).
645 15 Cho, W. K. *et al.* Mediator and RNA polymerase II clusters associate in
646 transcription-dependent condensates. *Science* **361**, 412-415,
647 doi:10.1126/science.aar4199 (2018).
648 16 Chong, S. *et al.* Imaging dynamic and selective low-complexity domain
649 interactions that control gene transcription. *Science* **361**,
650 doi:10.1126/science.aar2555 (2018).
651 17 Mir, M. *et al.* Dense Bicoid hubs accentuate binding along the morphogen
652 gradient. *Genes Dev* **31**, 1784-1794, doi:10.1101/gad.305078.117 (2017).

653 18 Nora, E. P. *et al.* Spatial partitioning of the regulatory landscape of the X-
654 inactivation centre. *Nature* **485**, 381-385, doi:10.1038/nature11049 (2012).
655 19 Mashtalir, N. *et al.* Modular Organization and Assembly of SWI/SNF Family
656 Chromatin Remodeling Complexes. *Cell*, doi:10.1016/j.cell.2018.09.032 (2018).
657 20 Charlop-Powers, Z., Zeng, L., Zhang, Q. & Zhou, M. M. Structural insights into
658 selective histone H3 recognition by the human Polybromo bromodomain 2. *Cell*
659 *Res* **20**, 529-538, doi:10.1038/cr.2010.43 (2010).
660 21 Slaughter, M. J. *et al.* PBRM1 bromodomains variably influence nucleosome
661 interactions and cellular function. *J Biol Chem* **293**, 13592-13603,
662 doi:10.1074/jbc.RA118.003381 (2018).
663 22 Porter, E. G. & Dykhuizen, E. C. Individual Bromodomains of Polybromo-1
664 Contribute to Chromatin Association and Tumor Suppression in Clear Cell Renal
665 Carcinoma. *J Biol Chem* **292**, 2601-2610, doi:10.1074/jbc.M116.746875 (2017).
666 23 Chen, J. *et al.* Single-molecule dynamics of enhanceosome assembly in
667 embryonic stem cells. *Cell* **156**, 1274-1285, doi:10.1016/j.cell.2014.01.062 (2014).
668 24 Ricci, M. A., Manzo, C., Garcia-Parajo, M. F., Lakadamyali, M. & Cosma, M. P.
669 Chromatin fibers are formed by heterogeneous groups of nucleosomes in vivo.
670 *Cell* **160**, 1145-1158, doi:10.1016/j.cell.2015.01.054 (2015).
671 25 Hassan, A. H., Neely, K. E. & Workman, J. L. Histone acetyltransferase
672 complexes stabilize swi/snf binding to promoter nucleosomes. *Cell* **104**, 817-827
673 (2001).
674 26 Ho, L. & Crabtree, G. R. Chromatin remodelling during development. *Nature* **463**,
675 474-484, doi:10.1038/nature08911 (2010).
676 27 Brownlee, P. M., Chambers, A. L., Oliver, A. W. & Downs, J. A. Cancer and the
677 bromodomains of BAF180. *Biochem Soc Trans* **40**, 364-369,
678 doi:10.1042/BST20110754 (2012).
679 28 Filippakopoulos, P. *et al.* Histone recognition and large-scale structural analysis
680 of the human bromodomain family. *Cell* **149**, 214-231,
681 doi:10.1016/j.cell.2012.02.013 (2012).
682 29 Kaeser, M. D., Aslanian, A., Dong, M. Q., Yates, J. R., 3rd & Emerson, B. M.
683 BRD7, a novel PBAF-specific SWI/SNF subunit, is required for target gene
684 activation and repression in embryonic stem cells. *J Biol Chem* **283**, 32254-32263,
685 doi:10.1074/jbc.M806061200 (2008).
686 30 Kakarougkas, A. *et al.* Requirement for PBAF in transcriptional repression and
687 repair at DNA breaks in actively transcribed regions of chromatin. *Mol Cell* **55**,
688 723-732, doi:10.1016/j.molcel.2014.06.028 (2014).
689 31 Moreira, J. M. & Holmberg, S. Transcriptional repression of the yeast CHA1 gene
690 requires the chromatin-remodeling complex RSC. *EMBO J* **18**, 2836-2844,
691 doi:10.1093/emboj/18.10.2836 (1999).
692 32 Van de Vosse, D. W. *et al.* A role for the nucleoporin Nup170p in chromatin
693 structure and gene silencing. *Cell* **152**, 969-983, doi:10.1016/j.cell.2013.01.049
694 (2013).
695 33 Strom, A. R. *et al.* Phase separation drives heterochromatin domain formation.
696 *Nature* **547**, 241-245, doi:10.1038/nature22989 (2017).
697 34 Harada, B. T. *et al.* Stepwise nucleosome translocation by RSC remodeling
698 complexes. *Elife* **5**, doi:10.7554/eLife.10051 (2016).

699 35 Nocetti, N. & Whitehouse, I. Nucleosome repositioning underlies dynamic gene
700 expression. *Genes Dev* **30**, 660-672, doi:10.1101/gad.274910.115 (2016).
701 36 Vazquez, J., Belmont, A. S. & Sedat, J. W. Multiple regimes of constrained
702 chromosome motion are regulated in the interphase Drosophila nucleus. *Curr Biol*
703 **11**, 1227-1239 (2001).
704 37 Chuang, C. H. *et al.* Long-range directional movement of an interphase
705 chromosome site. *Curr Biol* **16**, 825-831, doi:10.1016/j.cub.2006.03.059 (2006).
706 38 Clement, C. *et al.* High-resolution visualization of H3 variants during replication
707 reveals their controlled recycling. *Nat Commun* **9**, 3181, doi:10.1038/s41467-018-
708 05697-1 (2018).
709 39 Buckley, M. S. & Lis, J. T. Imaging RNA Polymerase II transcription sites in
710 living cells. *Current opinion in genetics & development* **25**, 126-130,
711 doi:10.1016/j.gde.2014.01.002 (2014).
712 40 Bulger, M. Hyperacetylated chromatin domains: lessons from heterochromatin. *J*
713 *Biol Chem* **280**, 21689-21692, doi:10.1074/jbc.R500004200 (2005).
714 41 Wang, Z. *et al.* Combinatorial patterns of histone acetylations and methylations in
715 the human genome. *Nat Genet* **40**, 897-903, doi:10.1038/ng.154 (2008).
716 42 Nakayama, T., Shimojima, T. & Hirose, S. The PBAP remodeling complex is
717 required for histone H3.3 replacement at chromatin boundaries and for boundary
718 functions. *Development* **139**, 4582-4590, doi:10.1242/dev.083246 (2012).
719 43 Kadoch, C. *et al.* Dynamics of BAF-Polycomb complex opposition on
720 heterochromatin in normal and oncogenic states. *Nat Genet* **49**, 213-222,
721 doi:10.1038/ng.3734 (2017).
722 44 Nakayama, R. T. *et al.* SMARCB1 is required for widespread BAF complex-
723 mediated activation of enhancers and bivalent promoters. *Nat Genet* **49**, 1613-
724 1623, doi:10.1038/ng.3958 (2017).
725 45 Nielsen, A. L. *et al.* Selective interaction between the chromatin-remodeling
726 factor BRG1 and the heterochromatin-associated protein HP1alpha. *EMBO J* **21**,
727 5797-5806 (2002).
728 46 Lavigne, M. *et al.* Interaction of HP1 and Brg1/Brm with the globular domain of
729 histone H3 is required for HP1-mediated repression. *PLoS Genet* **5**, e1000769,
730 doi:10.1371/journal.pgen.1000769 (2009).
731 47 Bosch-Presegue, L. *et al.* Mammalian HP1 Isoforms Have Specific Roles in
732 Heterochromatin Structure and Organization. *Cell Rep* **21**, 2048-2057,
733 doi:10.1016/j.celrep.2017.10.092 (2017).
734 48 Deaton, A. M. *et al.* Enhancer regions show high histone H3.3 turnover that
735 changes during differentiation. *Elife* **5**, doi:10.7554/eLife.15316 (2016).
736 49 Henikoff, S., Henikoff, J. G., Sakai, A., Loeb, G. B. & Ahmad, K. Genome-wide
737 profiling of salt fractions maps physical properties of chromatin. *Genome Res* **19**,
738 460-469, doi:10.1101/gr.087619.108 (2009).
739 50 Jin, C. & Felsenfeld, G. Nucleosome stability mediated by histone variants H3.3
740 and H2A.Z. *Genes Dev* **21**, 1519-1529, doi:10.1101/gad.1547707 (2007).
741 51 Jin, C. *et al.* H3.3/H2A.Z double variant-containing nucleosomes mark
742 'nucleosome-free regions' of active promoters and other regulatory regions. *Nat*
743 *Genet* **41**, 941-945, doi:10.1038/ng.409 (2009).

744 52 Verdin, E. & Ott, M. 50 years of protein acetylation: from gene regulation to
745 epigenetics, metabolism and beyond. *Nature reviews. Molecular cell biology* **16**,
746 258-264, doi:10.1038/nrm3931 (2015).
747 53 Roh, T. Y., Cuddapah, S. & Zhao, K. Active chromatin domains are defined by
748 acetylation islands revealed by genome-wide mapping. *Genes & development* **19**,
749 542-552, doi:10.1101/gad.1272505 (2005).
750 54 Bonev, B. & Cavalli, G. Organization and function of the 3D genome. *Nature*
751 *reviews. Genetics* **17**, 772, doi:10.1038/nrg.2016.147 (2016).
752 55 Serge, A., Bertaux, N., Rigneault, H. & Marguet, D. Dynamic multiple-target
753 tracing to probe spatiotemporal cartography of cell membranes. *Nat Methods* **5**,
754 687-694, doi:10.1038/nmeth.1233 (2008).
755 56 Normanno, D. *et al.* Probing the target search of DNA-binding proteins in
756 mammalian cells using TetR as model searcher. *Nat Commun* **6**, 7357,
757 doi:10.1038/ncomms8357 (2015).
758

759 **Acknowledgements**

760 We thank Y.J. Chen and C.S. Peng for development of initial Matlab scripts used for
761 SMT tracking. We are grateful to Z. Liu for providing the Matlab script and technical
762 advice for analysis of diffusion rates. We thank S. Healton for reagents and technical
763 assistance in acid extraction of histones, and J.C. Wheat for providing SAHA reagent and
764 initial aliquots of acetyl-H3 antibody. We also thank D. Shechter for providing the
765 histone H3 antibody. This work was supported by a grant from the NIH
766 (8U01DA047729-04, RAC and RHS) as part of the 4D Nucleome project, the NIH
767 (1R01GM126045-01, RAC) and a NIH Medical Scientist Training Program Grant
768 (T32GM007288, CAK).

769

770 **Author contributions**

771 Designed and supervised experiments: RAC, CAK, SHL, PC, WL, RHS

772 Generated material: CAK (cell lines, constructs), VW (cell lines, constructs), PD (cell
773 lines), LDL (JF dyes)

774 Performed experiments: CAK, SHL, PC, VW

Analyzed data: CAK, SHL, PC, VW, RAC, WL

Wrote paper: RAC, WL, CAK

Competing Interests

The authors declare no competing interests.

781 **Figure Legends**

782 **Figure 1: Spatial analysis of PBAF chromatin binding events using SMT to define**
783 **binding hubs and compartments.**

784 (**a**) Transcriptionally active genomic compartments (green) contain open chromatin
785 structures associated with acetylated histone marks (e.g. H3K27ac & H3K14ac) and the
786 H3.3 histone variant. Transcriptionally inactive genomic compartments (red) contain
787 closed chromatin structures associated with select methylated histone marks (e.g.
788 H3K27me^3 & H3K9me^3) and heterochromatic protein HP1α. PBAF contains multiple
789 bromodomains within the BAF180 subunit known to bind acetylated histone marks
790 associated with open chromatin compartments.

791 (**b**) Motion Blur HiLo microscopy (top panel) of a single U2OS cell stably expressing
792 Halo-BAF180 WT. PBAF containing Halo-BAF180 WT molecules that rapidly diffuse in
793 the nucleoplasm are blurred, while chromatin bound PBAF appears as single bright spots
794 (highlighted by red circles, lower panels). Disappearance of a spot (white arrow) is due to
795 unbinding or dissociation of PBAF from the chromatin.

796 (**c**) Strategy for measuring the non-homogeneous localization of PBAF chromatin binding
797 events in a nucleus. A 2D projection map of PBAF binding events (red dots) in the
798 nucleus over 18 minutes of imaging is shown. A grey box (left panel, zoomed view in the
799 right panel) outlines a representative window of PBAF binding events in a subnuclear
800 region. Binding events occurring within different sized windows (0.064 μm^2 [blue box]
801 and 2.54 μm^2 [black box], right panel) in this subnuclear region are counted as the
802 window is scanned over the nucleus. PBAF binding density is thereby determined by

803 counting the number of binding events located within a given size window. Scale bar, 2
804 μm.

805 (**d**) PBAF binding event frequency heat maps were obtained from two different scanning
806 sized windows using the 2D projection map in (**c**). Regions of high (red) and low (blue)
807 PBAF binding frequency is presented for the cell shown in (**c**). Top panels are zoomed in
808 views of dashed boxes in lower panels. PBAF hubs (top left panel, white box) were
809 identified as clusters of frequent PBAF chromatin binding to target loci. PBAF hubs were
810 grouped to form distinct compartments (right panels). Scale bar, 0.25 μm (top panels) and
811 2 μm (bottom panels), respectively.

812 **Figure 2: Spatial and temporal analysis of PBAF binding hubs**

813 (**a**) A schematic representation where PBAF cycles on and off an array of nucleosomes.

814 (**b**) Clustering analysis algorithms indicate PBAF binding events (red dots) within hubs
815 (left panel, blue outlines). The right panel displays an expanded inset of a boxed region in
816 the left panel.

817 (**c**) The number of hubs formed per cell, which express either wild-type PBAF WT or the
818 mutant PBAF ΔBD. N.S. = Not significant, p-value * = < 0.05 and ** = < 0.01. (N=39
819 WT DMSO cells, 17 ΔBD DMSO cells, 37 WT SAHA cells, and 22 ΔBD SAHA cells)

820 (**d**) Temporal occupancy of PBAF at a representative chromatin binding hub. Snapshots
821 of PBAF binding foci at different timepoints in movie (seconds) and the appearance of
822 PBAF binding highlighted by white boxes (top panel). The width of the black bars
823 represents the duration of individual PBAF/chromatin binding events in a hub (bottom

824 panel). White gaps represent latent time periods when the region containing a hub is not
825 occupied by PBAF. Timepoints (▲) from the top panel where PBAF binds in the hub.
826 Timepoints (△) where PBAF does not bind the hub.

827 (**e**) Median number of binding events per hub per cell (N=39 WT DMSO cells, 17 ΔBD
828 DMSO cells, 37 WT SAHA cells, and 22 ΔBD SAHA cells). N.S. = Not significant and
829 p-value * = < 0.05.

830 (**f**) The long latency time in PBAF binding hubs (N=39 WT DMSO cells, 17 ΔBD
831 DMSO cells, 37 WT SAHA cells, and 22 ΔBD SAHA cells). p-value ** = < 0.01 and
832 *** = < 0.001.

833 For data in panels (**c**), (**e**) and (**f**), the white bar in the solid black box is the median, while
834 the lower and upper boundaries of the black box correspond to the 25th and 75th
835 percentiles of the data respectively. Outliers typically represented less than 10% of the
836 dataset and therefore were omitted for clarity.

837 **Figure 3: Spatial analysis of high frequency PBAF binding, actively transcribing**
838 **H3.3 and heterochromatic HP1α compartments**

839 (**a**) Filtered heat map indicating regions of high PBAF chromatin binding frequency
840 shown in yellow and red for cells expressing wild-type Halo-BAF180 (i.e. WT, left panel)
841 and Halo-BAF180 ΔBD (i.e. ΔBD, right panel), respectively. Numbers of compartments
842 (yellow boxes) are indicated. The nucleus is outlined by a white dashed line. Scale bar =
843 2 μm.

844 (**b**) Filtered heat maps indicating regions of high frequency H3.3 and HP1α genomic
845 binding shown in yellow and red for cells expressing H3.3-SNAP (left panel) and SNAP-
846 HP1α (right panel), respectively. Yellow boxes highlight individual compartments. The
847 nucleus is outlined by a white dashed line. Scale bar = 2 μm.

848 (**c**) Median number of H3.3 and HP1α compartments in a cell expressing Halo-BAF180
849 wild-type (WT) or Halo-BAF180 ΔBD (ΔBD) (N=32 WT cells and N=31 ΔBD cells).

850 (**d**) Median size of H3.3 and HP1α compartments in a cell expressing Halo-BAF180
851 wild-type (WT) or mutant Halo-BAF180 ΔBD (ΔBD) (N=32 WT cells, 31 ΔBD cells).

852 For data shown in (**c**) and (**d**), the white bar in the solid black box is the median, while
853 the lower and upper boundaries of the black box correspond to the 25th and 75th
854 percentiles of the data respectively. (N=16 BAF180 WT/H3.3 cells, 16 BAF180
855 ΔBD/H3.3 cells, 16 BAF180 WT/ HP1α cells, and 15 BAF180 ΔBD/ HP1α cells). N.S. =
856 not significant, p value ** = < 0.01 and *** = <0.001. Outliers typically represented less
857 than 10% of the dataset and therefore were omitted for clarity.

858 **Figure 4: Spatial analysis of PBAF chromatin binding activities within H3.3 and**
859 **HP1α marked compartments**

860 (**a**) Overlap (blue) between areas of high binding frequency compartments for Halo-
861 BAF180 WT (orange) and either H3.3-SNAP (left panel, green) or SNAP-HP1α (right
862 panel, red). Scale bar, 2 μm.

863 (**b**) Quantification of total area within a cell (μm^2) for PBAF's chromatin binding
864 compartments (orange), transcriptionally active (H3.3, green, top panel) and
865 heterochromatic (HP1α, red, bottom panel) compartments. The percentage of overlaps
866 between compartments is indicated.
867 (**c**) Distribution of PBAF's total chromatin binding events within transcriptionally active
868 (H3.3, green, top panel) or heterochromatic (HP1α, red, bottom panel) compartments in a
869 cell. The percentage PBAF chromatin binding events within H3.3 or HP1α marked
870 compartments in a cell is indicated.
871 (**d**) Representative spatial distribution of PBAF's chromatin binding events (orange dot)
872 within a transcriptionally active H3.3 compartment (left panel) and a HP1α
873 heterochromatic compartment (right panel). The periphery of the H3.3 and HP1α
874 compartment is shown in green and red respectively. The scale bar is indicated.
875
876 (**e**) Spatial probability of wild-type PBAF (WT, top panels) and mutant PBAF ΔBD
877 binding events (bottom panels) distributed in either H3.3 (left) or HP1α (right)
878 compartments. N=16 WT/H3.3 cells, 16 ΔBD/H3.3 cells, 16 WT/ HP1α cells, and 15
879 ΔBD/ HP1α cells. N.S. = not significant, p value * = < 0.05, ** = < 0.01 and *** = <
880 0.001. The white bar present in the solid black box is the median, while the lower and
881 upper boundaries of the black box correspond to the 25th and 75th percentiles of the data,
882 respectively. Outliers typically represented less than 10% of the dataset and therefore
883 were omitted for clarity.

884 **Figure 5: Residence time analysis of chromatin-bound PBAF in distinct**
885 **compartments**

886 (**a**) Positions of PBAF tracks within transcriptionally active compartments were plotted
887 with residence times (color-coded based on duration) in the third dimension in a
888 representative cell. Compartment (C) identity is listed.

889 (**b**) 1−Cumulative Distribution Function Plot (1−CDF) of PBAF bound to chromatin in
890 compartment 4 (C4) from the cell presented in (**a**) was fitted to a single (gray dashed) or
891 two-component (red solid) exponential decay model. Fitting analysis of residence times
892 reveals two populations (i.e. stable and unstable) of PBAF that bound to chromatin.
893 Percentages of the stable and unstable binding populations are listed next to the residence
894 time.

895 (**c**) Stable residence time of PBAF bound to chromatin for H3.3 marked compartments 1-
896 9 (C1 to C9) from the cell presented in (**a**) is shown.

897 (**d**) Gaussian fits were generated to show the distribution of stable residence times of
898 chromatin bound wild-type PBAF (WT) within individual H3.3 (green bars, dark green
899 line) and HP1α (red bars, dark red line) compartments. (N=144 H3.3 marked
900 compartments from 16 Halo-BAF180 WT cells and N=114 HP1α marked compartments
901 from 16 Halo-BAF180 WT cells). Bin size = 2 seconds.

902 (**e**) Gaussian fits of the distribution of stable residence times of chromatin-bound mutant
903 PBAF BAF180 ΔBD within individual H3.3 (green bars, dark green line) and HP1α (red
904 bars, dark red line) compartments. (N=131 H3.3 marked compartments from 16 Halo-
905 BAF180 ΔBD cells, N=141 HP1α marked compartments from 16 Halo-BAF180 ΔBD
906 cells). Bin size = 2 seconds.

907 **Figure 6: Curvilinear movement analysis of chromatin bound PBAF**

908 (**a**) Euchromatin contains a low density of nucleosomes resulting in fast local diffusion of
909 chromatin bound PBAF (left panel). Heterochromatin contains densely packed
910 nucleosomes that restrict local diffusion of chromatin bound PBAF (right panel).

911 (**b**) Representative plots of two nearby PBAF chromatin binding events within similar
912 time frames displaying curvilinear directional non-brownian movement. Localizations
913 from individual PBAF binding trajectories (yellow and blue thin lines) were time-
914 averaged and highlighted (orange and dark blue thick lines). Frame to frame X, Y
915 displacements were measured from the beginning of the binding event (green dot) to the
916 end (red dot).

917 (**c**) A representative PDF plot showing PBAF's velocity of individual binding trajectories
918 within a nucleus. N=4362 binding trajectories in 16 PBAF WT cells. Across all
919 conditions, PDF plots were fit with multiple Gaussian models to segment four different
920 populations of distinct velocities (slow, medium, fast1, and fast2). The percentage for
921 each population is listed.

922 (**d**) Population distribution of velocities for chromatin bound PBAF WT or mutant PBAF
923 ΔBD within H3.3 or HP1α compartments. The percentage for each population of PBAF's
924 velocity (i.e. fast, medium and slow) within the same compartment is presented. N=549
925 binding trajectories of PBAF WT inside H3.3 compartments from 16 cells. N=527
926 binding trajectories of PBAF WT inside HP1α compartments from 16 cells. N=613
927 binding trajectories of the mutant PBAF ΔBD inside of H3.3 compartments from 16 cells.

928 N=787 binding trajectories of the mutant PBAF ΔBD inside HP1α compartments from 15
929 cells.

930 **Figure 7: Models of PBAF's dynamic chromatin targeting to shape genome**
931 **organization.**

932 (**a**) Highly localized histone acetylation in hubs and compartments increases PBAF's
933 association, revisiting and anchored binding via BAF180 bromodomains. Removal of
934 PBAF's bromodomains decreases residence time (elevated k_{off}) in compartments and
935 increases latency between binding events (reduced k_{on}) in hubs.

936 (**b**) PBAF helps to shape H3.3 compartments by binding to boundary elements at the
937 periphery to prevent invasion of heterochromatin into transcriptionally active
938 compartments. In H3.3 rich euchromatic compartments, less stable chromatin results in
939 PBAF binding for a shorter duration of time than within stable HP1α rich
940 heterochromatin. PBAF's residence time on chromatin is proportional to chromatin
941 stability. The velocity of genomic bound PBAF is decreased in densely packed
942 heterochromatin relative to H3.3 rich chromatin. Therefore, PBAF's velocity may reflect
943 chromatin compaction surrounding target nucleosomes.

944

Figure 1

Kenworthy_Fig. 1

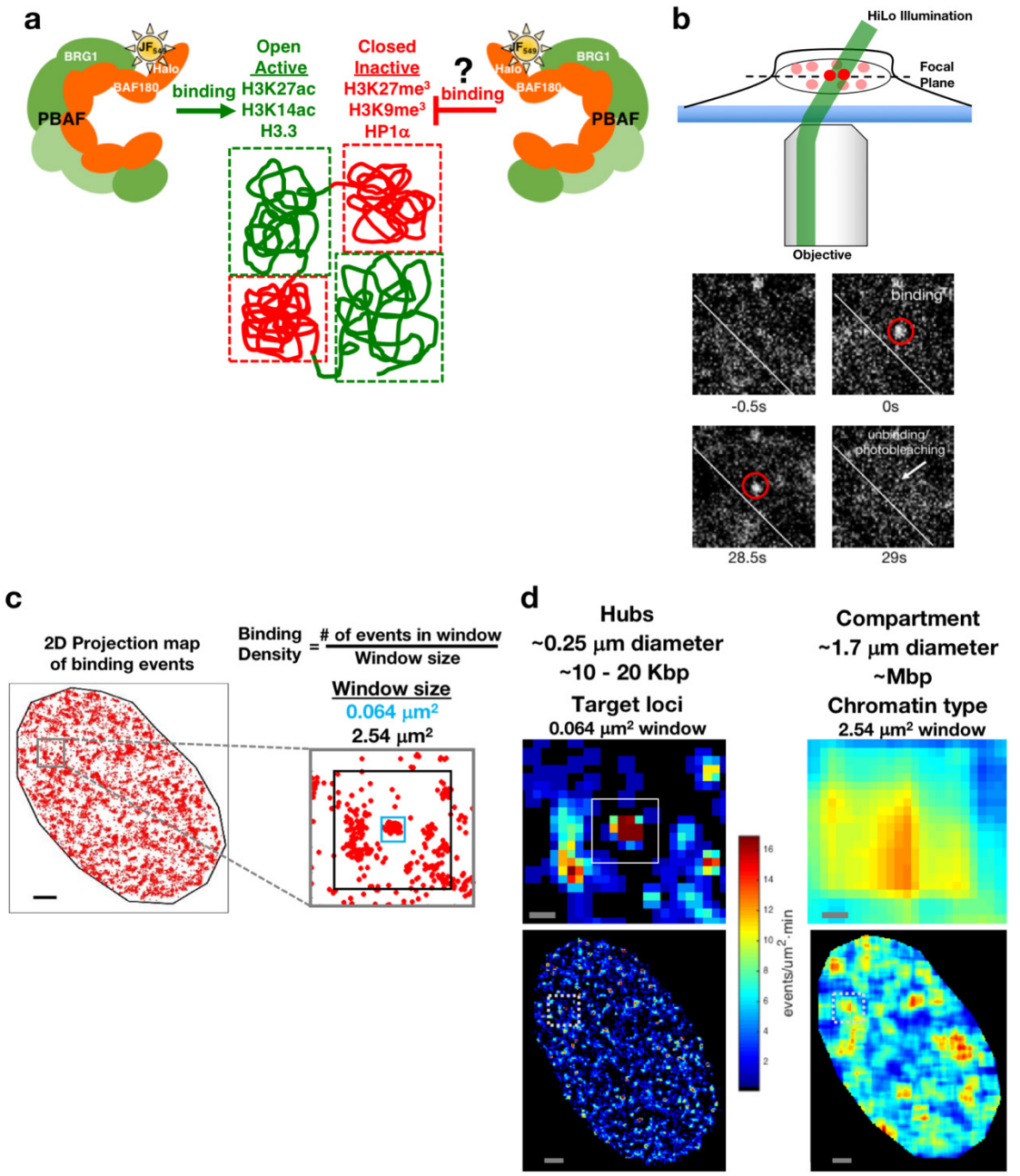

945

Figure 2 **Kenworthy_Fig. 2**

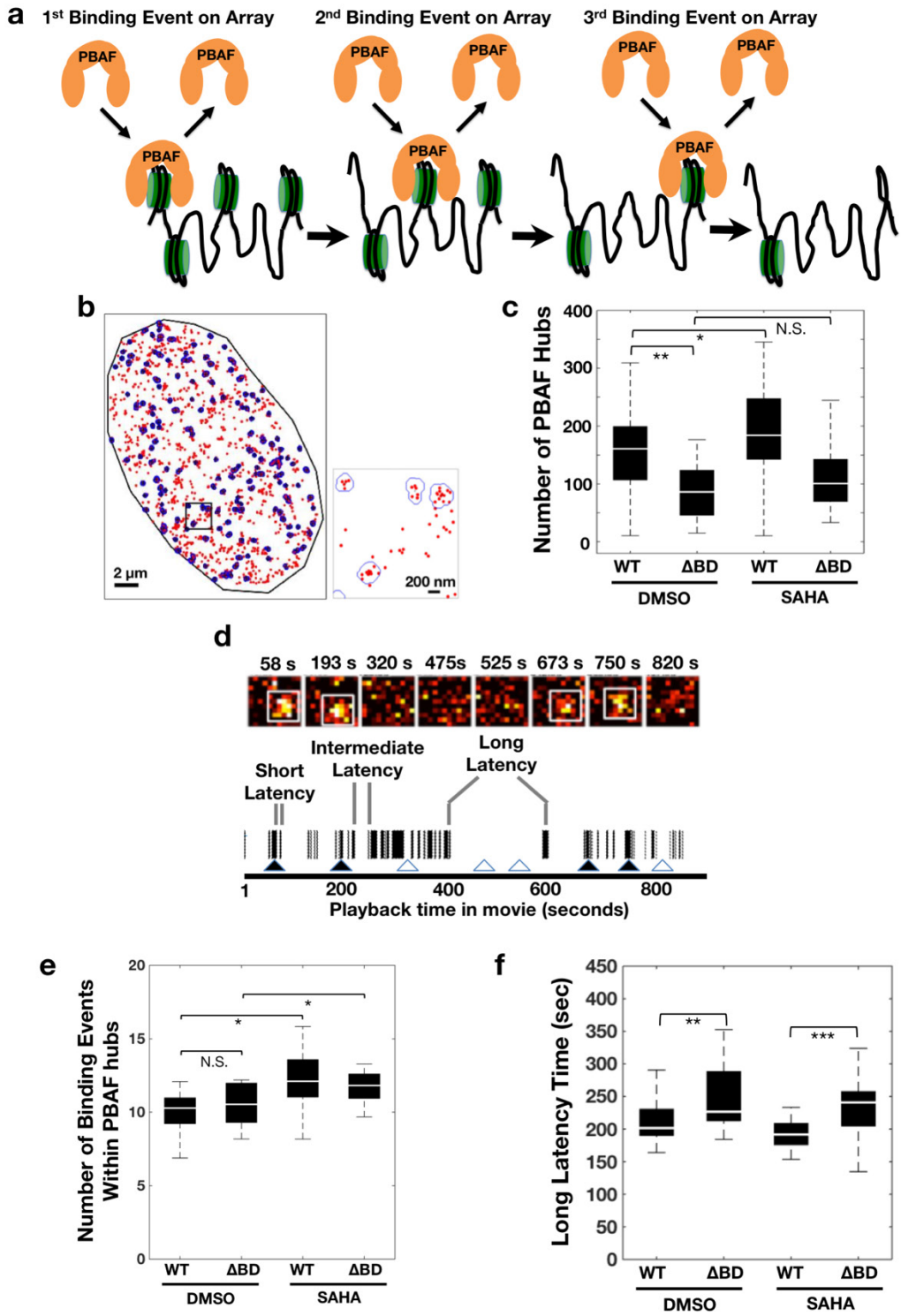

946

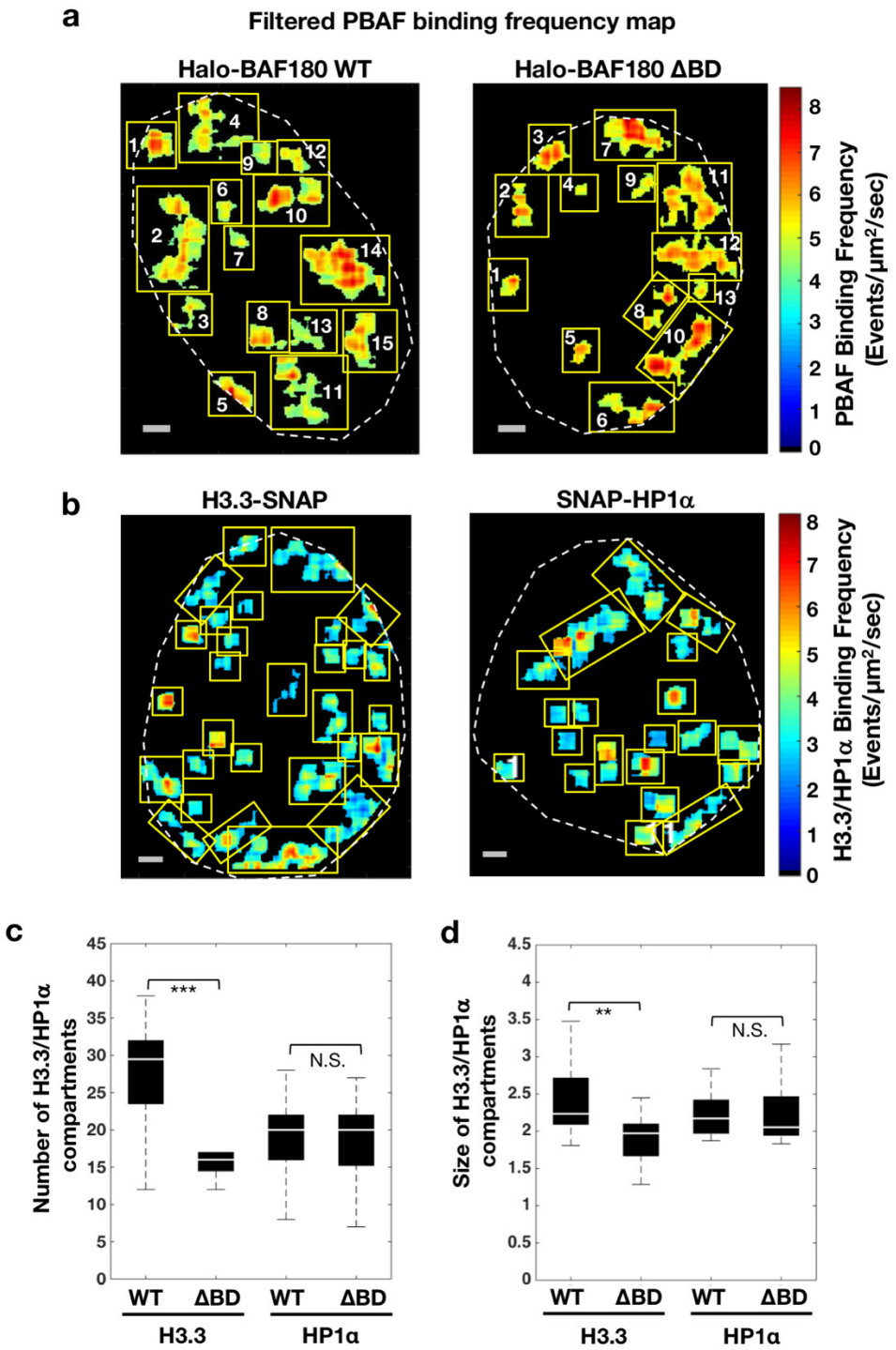
a
Filtered PBAF binding frequency map
Halo-BAF180 WT
Halo-BAF180 ΔBD
PBAF Binding Frequency (Events/μm²/sec)
b
H3.3-SNAP
SNAP-HP1α
H3.3/HP1α Binding Frequency (Events/μm²/sec)
c
Number of H3.3/HP1α compartments
***
N.S.
WT
ΔBD
WT
ΔBD
H3.3
HP1α
d
Size of H3.3/HP1α compartments
**
N.S.
WT
ΔBD
WT
ΔBD
H3.3
HP1α

947

Figure 4 **Kenworthy_Fig. 4**

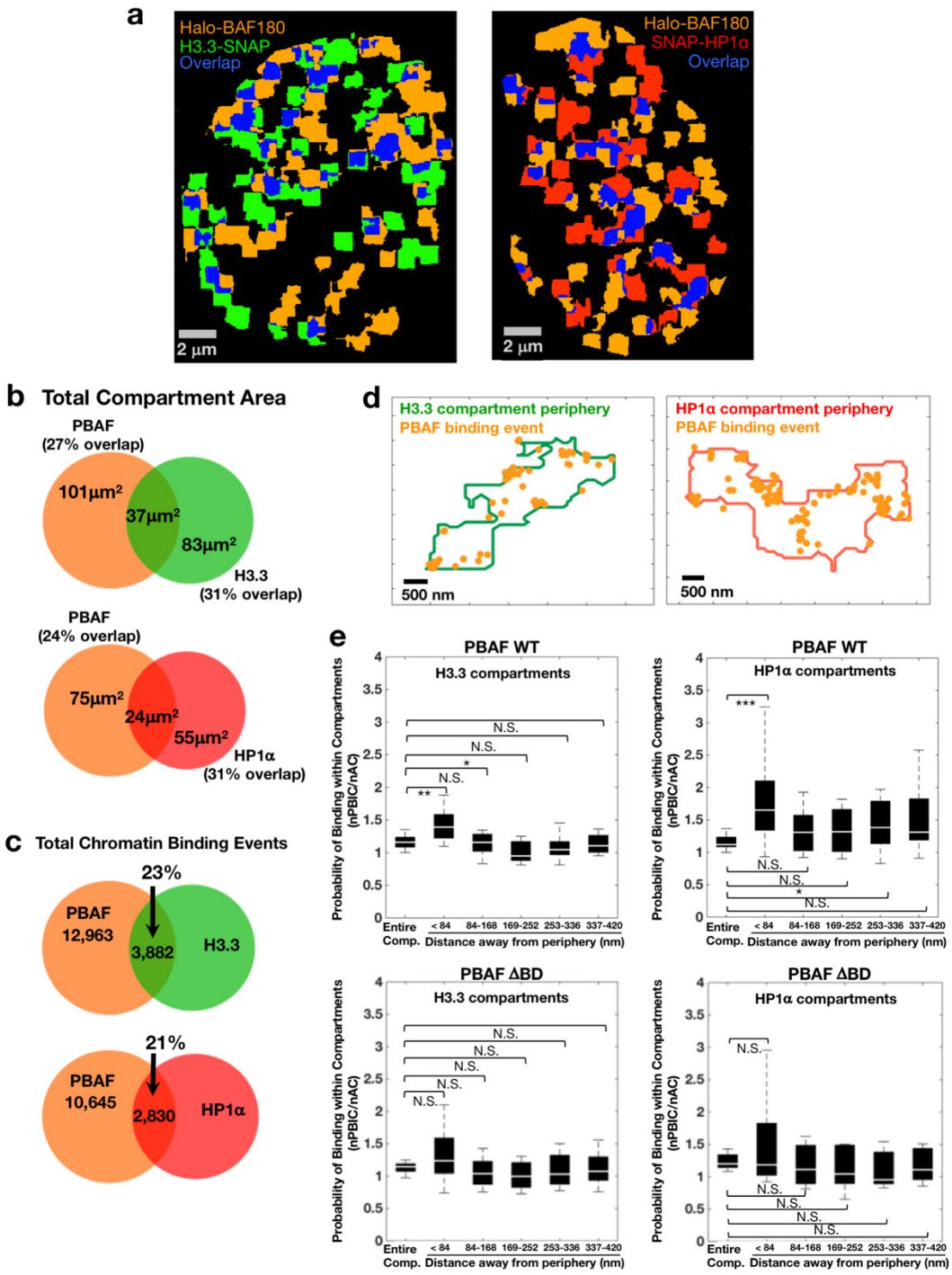

948

Figure 5

Kenworthy_Fig. 5

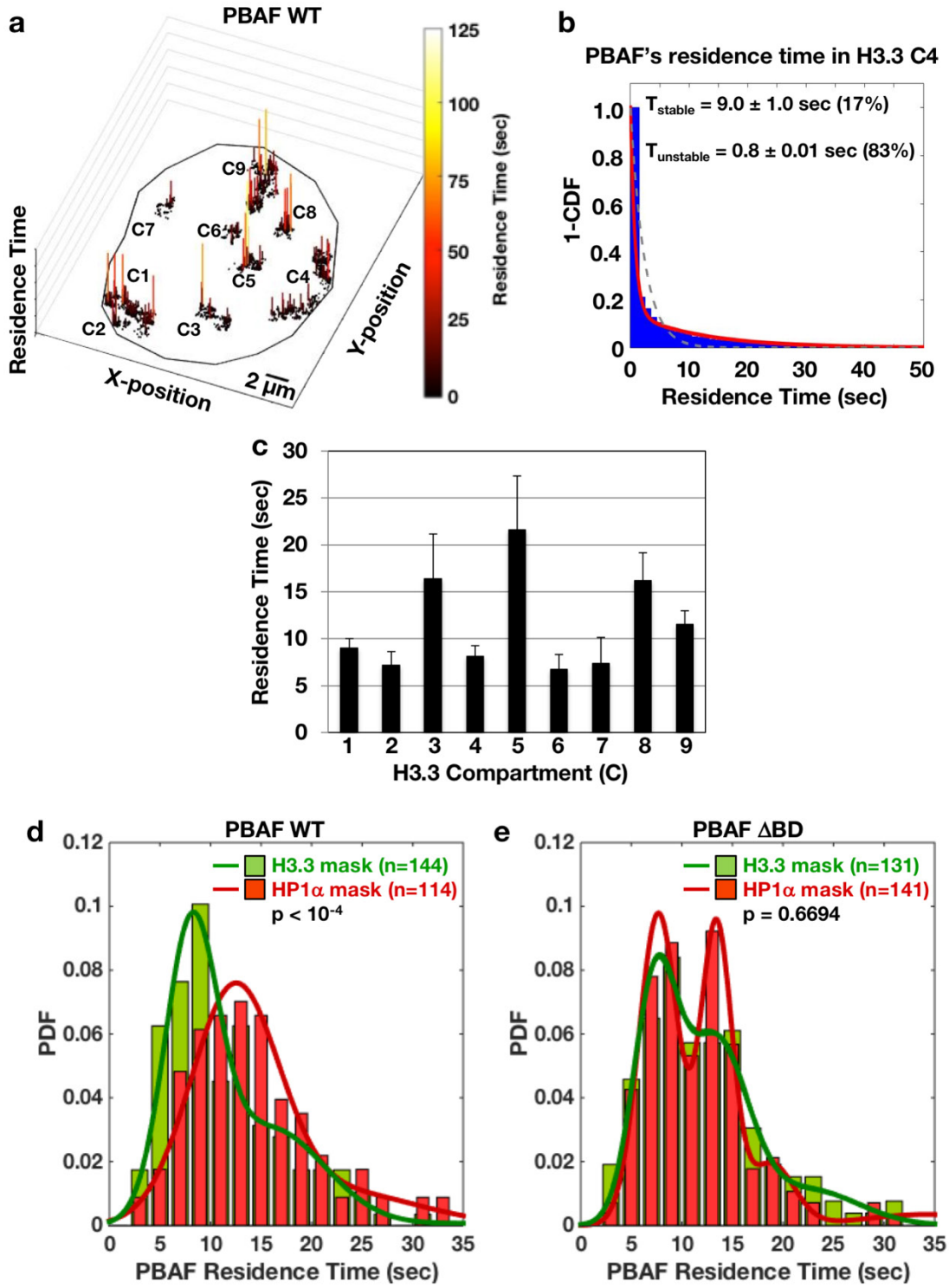

949

Figure 6 Kenworthy Fig. 6

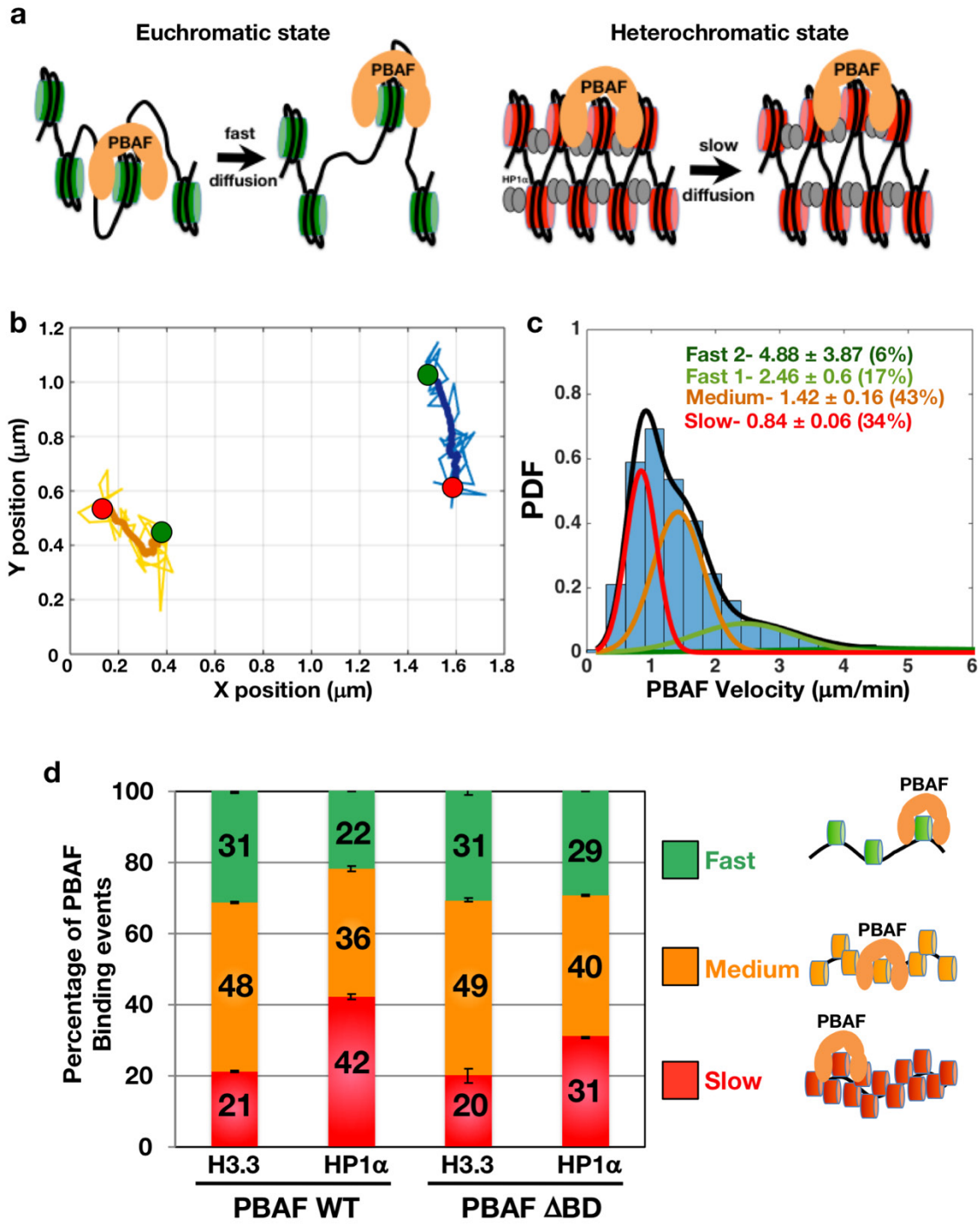

950

Figure 7 Kenworthy_Fig. 7

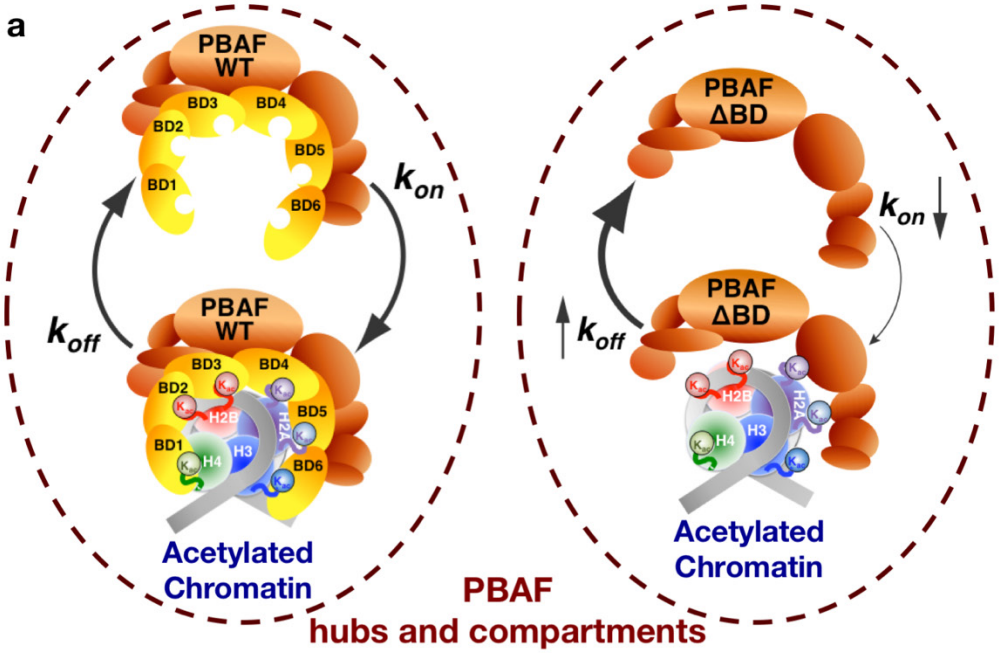

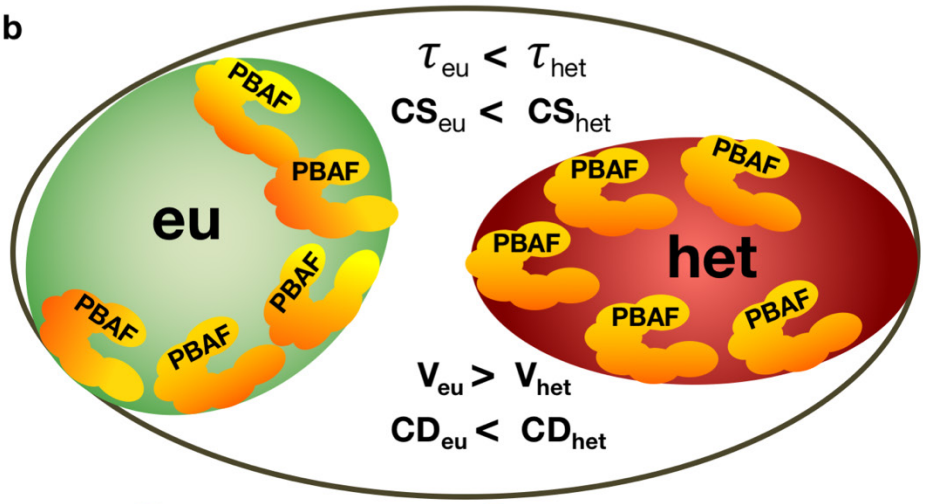

eu H3.3 Euchromatin het HP1α Heterochromatin

PBAF residence time (τ) $\propto$ Chromatin stability (CS)

PBAF Velocity (V) $\propto$ Chromatin density (CD)

951